

Diurnal Selective Radiative Cooling Impact in Mitigating Urban Heat Island Effect

Jaafar Younes, Kamel Ghali, Nesreen Ghaddar*

Department of Mechanical Engineering, American University of Beirut, Beirut 1107 2020, Lebanon



ARTICLE INFO

Keywords:

Urban heat island
radiative cooling
selective radiative properties
microclimate modeling

ABSTRACT

This study investigates the impact of diurnal radiative cooling (RC) roof panels RC roofs in mitigating the urban heat island (UHI) at city scale in comparison with high albedo roofs and concrete roofs. A validated microclimate model that embeds a building energy model is used to predict the street level temperature and thermal comfort. The effective radiative properties of RC surface are calculated using their spectral angular properties in a spectral angular atmospheric model. A case study of Beirut city with its morphology and microclimate was simulated on representative days of the year.

At the peak of a humid summer day in Beirut, daytime RC roof panels resulted in a reduction in air temperature at the pedestrian level by at least 0.8°C in high building density regions enhancing outdoor thermal comfort. While the RC panel's surface temperature drop was greatest at night, its effect on the microclimate at night was negligible. At lower humidity days, the RC surface temperature was lower, however, RC impact on pedestrian level air temperature was not significantly changed. At moderate and high humidity days, RC panels yielded a similar microclimate influence on pedestrian level air temperature and outdoor thermal comfort to high-performance cool roofs.

1. Introduction

Urban areas are continuously growing in size and population. In 2018, it was reported that 55% of the world's population lived in urban areas. This number is expected to increase to 68% by 2050 (Nations, 2018). The urbanization process induces regional climate modifications, and the modified climate is named the "urban climate". By comparing urban climates to surrounding climates, higher temperatures are observed in a phenomenon that has become known as the Urban Heat Island (UHI) effect (Landsberg, 1981). UHI effect has been reported in more than 400 cities around the world (Matthaios Santamouris, 2018). The major causes of UHI in cities include high anthropogenic heat releases and high radiant energy absorption and storage in massive urban structures (Carlosena et al., 2020). In light of the present global warming trend and fast urbanization, UHI has a significant impact on the quality of life of people and the sustainable development of cities (Bonafoni, Baldinelli, & Verducci, 2017; Guo et al., 2020). For instance, as air

temperature of a city rises, the cooling loads of buildings increase, resulting in higher energy consumption and higher peak electricity demand in that city. (Coutts, Daly, Beringer, & Tapper, 2013; Kolokotsa, Santamouris, & Zerefos, 2013; Mattheos Santamouris, Ding, & Osmond, 2019). Furthermore, UHI has a negative influence on the thermal comfort of urban residents. (Ghali, Ghaddar, & Bizri, 2011; Mirzaei, 2015).

Researchers proposed mitigation strategies and technologies to alleviate this phenomenon, such as minimizing anthropogenic heat releases, increasing vegetation, making buildings more efficient through using high albedo roofs (Rizwan, Dennis, & Chunho, 2008), and mist cooling (Ishii, Tsujimoto, Yoon, & Okumiya, 2009). Many studies have assessed the potential of cool roofs in mitigating UHI (Akbari & Kono-packi, 2004; Coutts et al., 2013; Kolokotsa et al., 2013; Yang et al., 2018) and found that reduced absorbed solar radiation results in a decreased cooling load. In direct sunlight exposure, however, cool roofs usually suffer from a positive thermal balance, restricting the lowest temperature they can achieve by the ambient air temperature, even though a

Abbreviations: BEM, Building Energy Model; ECMWF, European Centre for Medium-Range Weather Forecasts; ERA5, Fifth generation of the atmospheric reanalysis for the global climate; GBA, Greater Beirut Area; RC, Radiative cooling; SMARTS, Simple Model of the Atmospheric Radiative Transfer of Sunshine; SRTM, Nasa's Shuttle Radar Topography Mission; TEB, Town Energy Balance; UCM, Urban Canopy Model; UHI, Urban Heat Island; UTCI, Universal Thermal Climate Index; WPTherm, William Paterson University's tool for Thermal Energy and Radiation management with multi-layer nanostructures.

* Corresponding author: Nesreen Ghaddar.

E-mail address: farah@aub.edu.lb (N. Ghaddar).

Nomenclature	
AM	Air mass coefficient [-]
I_{bb}	Blackbody spectral intensity [$\text{W}/\text{m}^2 \cdot \text{sr} \cdot \mu\text{m}$]
Q_{atm}	Absorbed atmospheric flux [W/m^2]
$Q_{emitted}$	Emitted radiation flux [W/m^2]
Q_{net}	Net radiative flux [W/m^2]
$Q_{non-Radiative}$	Non-radiative heat fluxes [W/m^2]
Q_{solar}	Absorbed solar flux [W/m^2]
RH	Relative humidity [%]
T_s	Surface temperature [k]
T_{dew}	Dew temperature of Air [$^\circ\text{C}$]
$\bar{\alpha}_{atm}$	Effective absorptivity to atmospheric radiation [-]
$\bar{\alpha}_{sw}$	Effective hemispherical shortwave absorptivity [-]
ΔT_{air}	Drop in air temperature at pedestrian level [$^\circ\text{C}$]
$\Delta UTCI$	Drop in the Universal Thermal Climate Index [$^\circ\text{C}$]
ΔT	Temperature difference [$^\circ\text{C}$]
ε	Spectral directional emissivity [-]
$\bar{\varepsilon}$	Effective hemispherical emissivity [-]
ε_{atm}	Spectral directional atmospheric emissivity [-]
ϕ	Azimuthal angle [rad]
λ	Wavelength [μm]
θ	Zenith angle [rad]
σ	Stefan–Boltzmann constant [$\text{W}/\text{m}^2 \cdot \text{k}^4$]

<i>Greek Symbols</i>	
α	Spectral directional absorptivity [-]

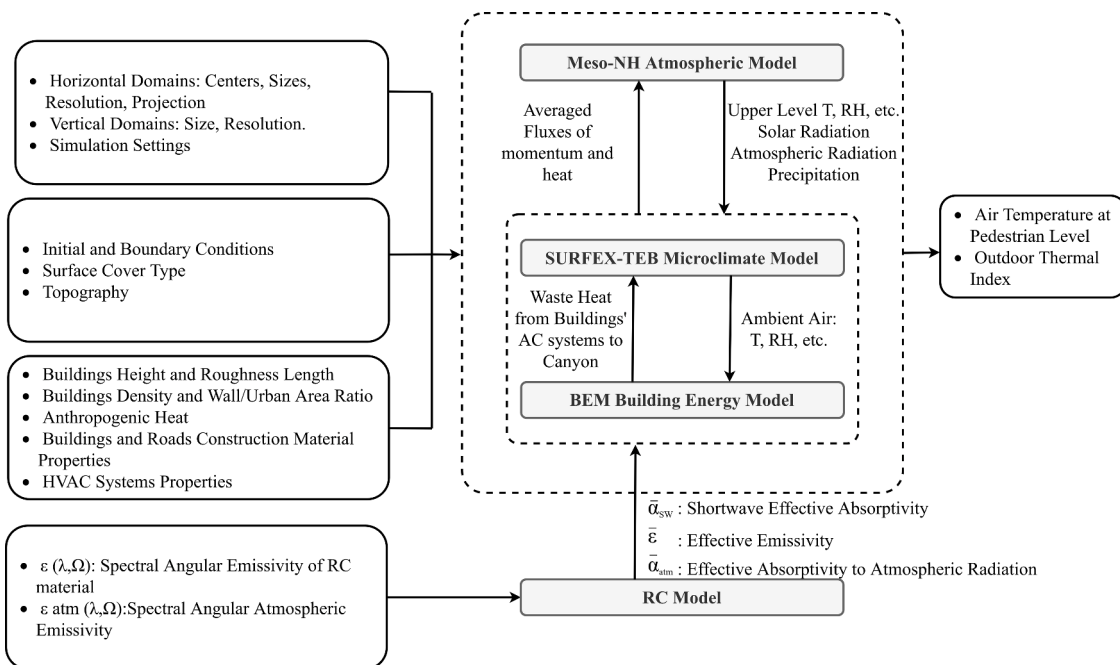


Fig. 1. The integration of models used to simulate the influence of RC roof panels on UHI, as well as their inputs and outputs.

large portion of the incident solar radiation is reflected. Mist cooling, on the other hand, allows for a lower air temperature than the original ambient temperature in particular settings. However, the decrease in the temperature of air comes at the expense of its humidity, which is a key parameter in human comfort. Moreover, using water is not a cost-effective solution in some regions. The question that arises is: would it be possible to achieve a temperature lower than ambient without using water given the new developments in radiative cooling (RC) materials?

By combining high shortwave reflectivity with selective emissivity, newly developed daytime RC materials are reported to provide passive cooling and achieve sub-ambient temperatures under direct sunlight exposure (Raman, Abou Anoma, Zhu, Rephaeli, & Fan, 2014; Zhai et al., 2017). RC materials have high emissivity in the atmospheric transparency window, and they have low absorptivity outside it (*the transparency window is the spectral range between 8 and 13 μm where the atmosphere has low emissivity /absorptivity*) (Gentle, Aguilar, & Smith, 2011; Trombe, 1975). This fact minimizes absorbed atmospheric radiation and allows such materials to emit radiant energy into the outer sky

without being trapped by atmospheric gases. The characteristics of RC materials make installing them on rooftops promising in terms of reducing the amount of energy absorbed by urban structures. Moreover, throughout the cooling season, a reduction is expected in buildings' cooling loads and their associated anthropogenic heat discharged into the urban environment, which may lead to a reduction in the UHI effect. Radiative cooling has gained high research interest recently. For instance, Feng et al. (Feng, Khan, Doan, Gao, & Santamouris, 2021) have studied the heat mitigation potential of broadband radiative coolers on a city scale. Nevertheless, the angular and spectral emissivity characteristics of selective radiative coolers make integrating them with city scale models challenging. To the authors' knowledge, the heat mitigation potential of such selective radiative coolers on the microclimate air temperature of a city, has not been addressed in the literature.

Modeling of UHI has commonly been performed using urban canopy models (UCMs) coupled to mesoscale atmospheric models (Li & Norden, 2016; Masson, 2000). Many UHI mitigation measures, including cool roofs, have been assessed using these models. The broad band emissivity and surface albedo should be provided in conventional

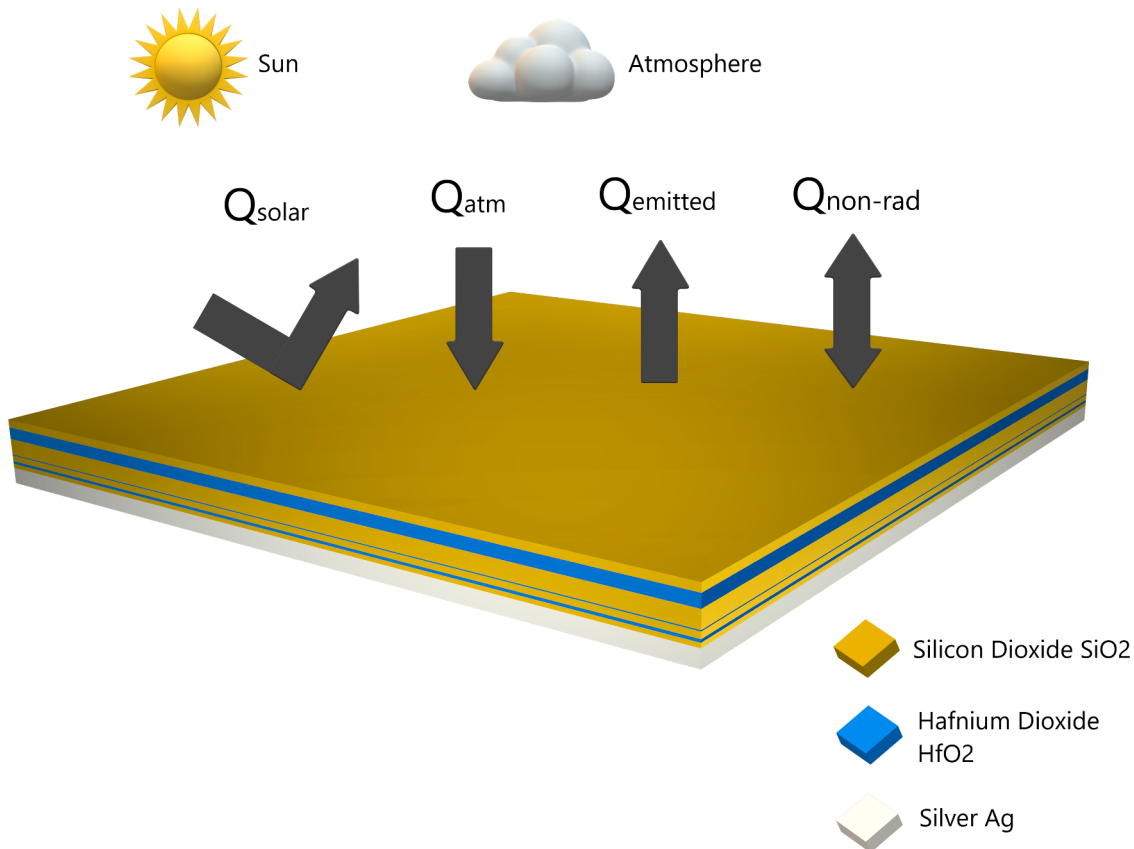


Fig. 2. Sketch for thermal fluxes at a typical RC material (Raman's).

Table 1

Horizontal domains of simulation: size, resolution, and number of points.

Domain	Size	Resolution	Number of Points
Outermost Domain D1	1200 km x 1200 km	8 km	150 x 150
Intermediate Domain D2	200 km x 200 km	2 km	100 x 100
Innermost Domain D3	16 km x 16 km	500 m	32 x 32

MESO-NH - TEB simulations. However, with selective RC panels, this is not straightforward for two reasons: The radiative properties of the RC panels are angular and spectral with high emissivity in the atmospheric window and the atmospheric emitted radiation is also angular and spectral with low emissivity in that window. The combined spectral radiative characteristics of the surface and atmosphere make implementing RC panels into microclimate simulation models challenging. Thus, the novelty of this study is in the development of an approach for modeling and incorporating RC roof panels in city-scale models and analyzing their impact on UHI at city scale. This is accomplished by including the effect of RC panels in the energy balance of roofs in a building energy model that is coupled to a town microclimate model and an atmospheric model. The impact of RC panels is studied under different humidity conditions and compared to the impact of cool roofs which are conventionally deployed for UHI mitigation. The models are applied to a case study for the city of Beirut during different seasons spanning moderately dry and moderately humid weather. The effect of RC panels on pedestrian air temperature and associated outdoor thermal comfort is predicted and compared to that of cool roofs.

2. Methodology

Four models are needed to study the impact of RC roof panels on UHI: (i) an RC model that simulates various fluxes across the RC layer

(ii) a building energy model that captures the decrease in cooling load due to RC, (iii) a microclimate model to capture the effect on microclimate air temperature, and (iv) an atmospheric model that allows exchanging momentum and thermal fluxes between the atmosphere and the microclimate model. In the present study, the energy balance model presented by Raman et al. (Raman et al., 2014) is adopted to model the RC roof layer, the Town Energy Balance (TEB) and its embedded Building Energy Model (BEM) are adopted as microclimate and building energy models, respectively, and Meso-NH is adopted as an atmospheric model (Masson, 2000).

2.1. Urban microclimate model

Fig. 1 shows the interaction between different models used to simulate the influence of RC roof panels on UHI as well as their inputs and outputs. The atmospheric model Meso-NH provides the coupled surface model, SURFEX, with meteorological information that serves as its upper-level boundary conditions (Moigne, 2012). Simultaneously, SURFEX provides Meso-NH with heat and momentum fluxes that serve as its lower boundary conditions. SURFEX has multiple sub-models to account for different surface types, the Town Energy Balance TEB is its sub-model for urban areas. Using the canyon approach, TEB represents urban areas as opposing buildings separated by a single canyon (Masson, 2000). To simulate microclimates, TEB requires inputs including urban geometry, construction material properties, and anthropogenic heat released into the town, in addition to meteorological conditions provided by Meso-NH (see Fig. 1). The main sources of anthropogenic heat in cities are vehicles, industries, and buildings (Sailor & Lu, 2004). While heat fluxes from vehicles and industries are external inputs to the model, the heat released from buildings is computed via the embedded Building Energy Model (BEM) (Masson, 2000). Since BEM considers the energy budget of the roof while computing the cooling loads, it can

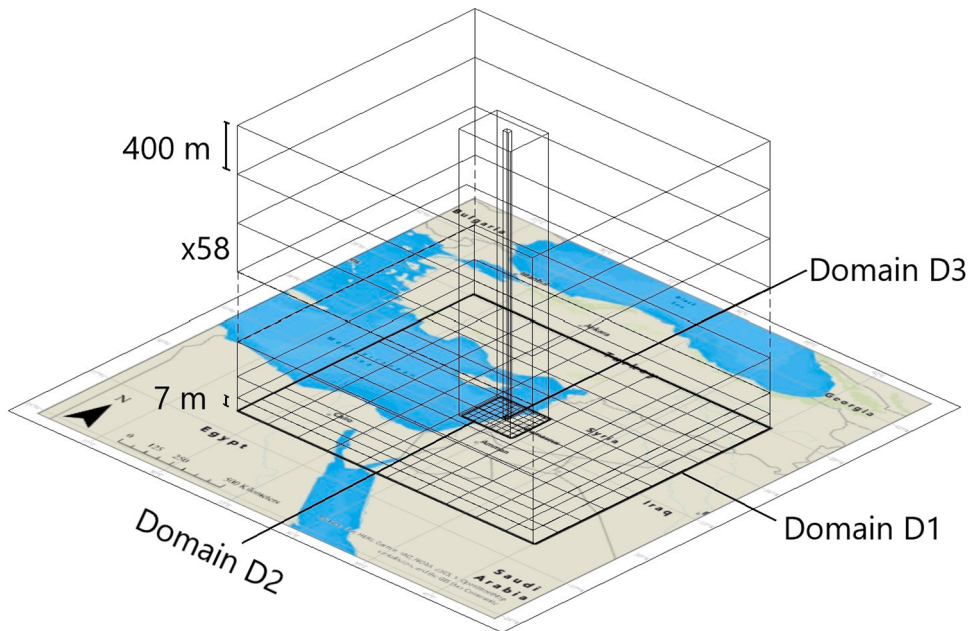


Fig. 3. Horizontal domains of simulation: outermost domain D1, intermediate domain D2, innermost domain D3 and the vertical stretching grid.

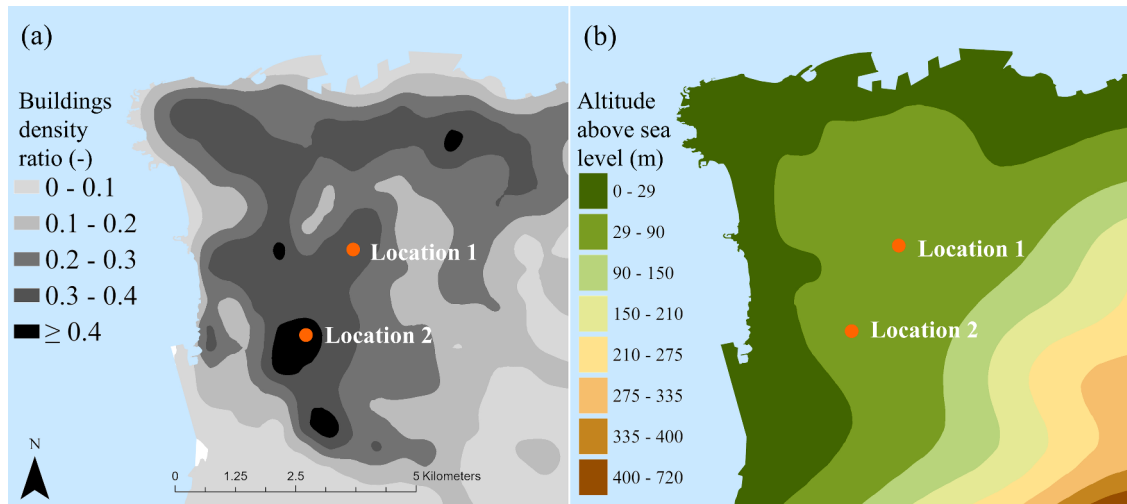


Fig. 4. (a) building density ratio (-) in the innermost domain D3 obtained via city's GIS data and (b) Altitude above sea level (m) in the innermost domain D3 obtained by SRTM database.

capture the effect of adding an RC layer to the rooftop. Because of the added RC layer, the cooling loads in buildings are reduced, and anthropogenic heat released into the microclimate by air conditioning (AC) systems is decreased, resulting in a decrease in microclimate air temperature. To assess the influence of RC panels on UHI intensity, the predicted air temperature at the pedestrian level when RC is integrated is compared to a baseline case where the roof is composed of typical construction.

2.2. The RC model and its integration with the urban microclimate model

Fig. 2 shows the thermal fluxes for a typical multilayer radiative cooler facing the sky. The silver layer in the figure is responsible for the shortwave reflectivity, and the upper alternating layers correspond to the selective emissivity of the material. Using the energy balance model presented by Raman et al. (Raman et al., 2014), the net cooling flux Q_{net} of the RC layer with a sky view factor of unity can be expressed as

$$Q_{\text{net}} = Q_{\text{emitted}} - Q_{\text{solar}} - Q_{\text{atm}} - Q_{\text{non-rad}} \quad (1)$$

where the terms on the right side of the equation of equation (1) are Q_{emitted} : the radiation flux emitted from the surface; Q_{solar} : the shortwave solar radiation flux absorbed by the layer; Q_{atm} : the longwave atmospheric radiation flux absorbed by the layer; and $Q_{\text{non-rad}}$: the non-radiative heat fluxes between the layer and its surroundings. Surfaces within TEB are assumed to have broadband emissivity in line with the degree of various approximations in the model (Moigne, 2012). However, the spectral and directional features of RC panels are essential for their modeling. To resolve this issue in the TEB model, an RC model and a spectral atmospheric model were used to determine the following:

- i) The RC material effective emissivity ($\bar{\epsilon}$) from its spectral directional emissivity ($\epsilon(\lambda, \theta)$).
- ii) The RC material effective absorptivity to atmospheric radiation ($\bar{\alpha}_{\text{atm}}$) from its spectral directional absorptivity ($\alpha(\lambda, \Omega)$) and the

Table 2
Data acquired from databases for the simulation, summarized.

Input	Source	Data
Surface Cover	ECOCLIMAP-II	proportion of different cover types in studied domain
Clay and Sand Maps	Harmonized World Soil Database (HWSD)	Soil texture
Topography	NASA Shuttle Radar Topography Mission (SRTM)	Altitude of surface above sea level
Atmospheric Model Boundary and Initial Conditions	European Centre for Medium-Range Weather Forecasts (ECMWF, 2021) – fifth generation of the atmospheric re-analysis for the global climate (ERA5)	Invariant Data: Geopotential, Land-sea mask Surface Data: Snow depth, Soil temperature at different levels, volumetric soil water – different layers Model Level Data: Logarithm of surface pressure, specific humidity, temperature, wind velocity

spectral directional emissivity of the atmosphere ($\varepsilon_{\text{atm}}(\lambda, \Omega)$). $\bar{\alpha}_{\text{atm}}$ indicates how much radiation emitted from the atmosphere is absorbed by the RC surface.

iii) The RC material effective shortwave absorptivity ($\bar{\alpha}_{\text{sw}}$) from $\alpha(\lambda, \Omega)$ in the shortwave range.

Due to the limited surface temperature variation for RC applications, $\varepsilon(\lambda, \theta)$ is assumed independent on temperature (Raman et al., 2014) and hence $\bar{\varepsilon}$ can be assumed independent. As for $\varepsilon_{\text{atm}}(\lambda, \Omega)$, it is represented in literature as being dependent on the dew temperature of air (T_{dew}) and on day-night effect (Berger & Bathiebo, 1989). Berger's atmospheric model (Berger & Bathiebo, 1989) and Granqvist's equation (Granqvist & Hjortsberg, 1981) are used to calculate $\varepsilon_{\text{atm}}(\lambda, \theta)$ for the range of T_{dew} faced throughout each simulation run at day and at night. T_{dew} fluctuation can be determined using either measured data from the simulation domain or the result of an initial simulation run. The mean value of $\bar{\alpha}_{\text{atm}}$ was then used after making sure that the maximum deviation from the mean in each simulation run is small.

According to Kirchhoff's law of radiation, $\alpha(\lambda, \Omega)$ is considered equal to $\varepsilon(\lambda, \theta)$ (Kirchhoff, 1978), hence $\varepsilon(\lambda, \theta)$ and $\varepsilon_{\text{atm}}(\lambda, \Omega)$ are enough to calculate the three effective parameters as shown in Fig. 1. Once the three parameters: $\bar{\varepsilon}$, $\bar{\alpha}_{\text{atm}}$, and $\bar{\alpha}_{\text{sw}}$ are determined, they are implemented into the roof energy balance equation of BEM via source code change. The parameter $\bar{\varepsilon}$ can be computed by integrating $Q_{\text{emitted}}(T_s, \lambda)$ over the entire wavelength range divided by the blackbody emission obtained by Stefan–Boltzmann equation:

$$\bar{\varepsilon} = \frac{\int_0^{\infty} \int_0^{2\pi} \int_0^{\frac{\pi}{2}} I_{\text{bb}}(T_s, \lambda) \varepsilon(\lambda, \theta) \cos\theta \sin\theta d\theta d\phi d\lambda}{\sigma T_s^4} \quad (2)$$

where θ and ϕ are the zenith and azimuthal angles respectively, I_{bb} is the well-known blackbody spectral intensity, and σ is the Stefan–Boltzmann constant.

As for $\bar{\alpha}_{\text{atm}}$, since the atmospheric emittance is majorly emitted from the near ground atmosphere where water vapor and carbon dioxide are strongly absorbing (Zhao et al., 2019), it is commonly modeled in

literature as the product of $\varepsilon_{\text{atm}}(\lambda, \Omega)$ and the radiance of a blackbody at ambient temperature $I_{\text{bb}}(T_{\text{amb}}, \lambda)$ (Carlosena et al., 2020; Raman et al., 2014; Zhao et al., 2019). The spectrum of a blackbody lies in the mid- and far- infrared regions (Zhao et al., 2019) between 3 and 60 μm . Hence $\bar{\alpha}_{\text{atm}}$ can be computed by dividing the absorbed atmospheric radiation Q_{atm} by the emitted atmospheric radiation in that range:

$$\bar{\alpha}_{\text{atm}} = \frac{\int_{3 \mu\text{m}}^{60 \mu\text{m}} \int_0^{2\pi} \int_0^{\frac{\pi}{2}} I_{\text{bb}}(T_{\text{amb}}, \lambda) \varepsilon_{\text{atm}}(\lambda, \Omega) \varepsilon(\lambda, \Omega) \cos\theta \sin\theta d\theta d\phi d\lambda}{\int_{3 \mu\text{m}}^{60 \mu\text{m}} \int_0^{2\pi} \int_0^{\frac{\pi}{2}} I_{\text{bb}}(T_{\text{amb}}, \lambda) \varepsilon_{\text{atm}}(\lambda, \Omega) \cos\theta \sin\theta d\theta d\phi d\lambda} \quad (3)$$

As for the solar absorbed radiation, the air mass (AM) coefficient is commonly used to characterize the solar spectrum after sunlight travels through atmosphere (Zhao et al., 2019). Hence, the effective hemispherical shortwave absorptivity ($\bar{\alpha}_{\text{sw}}$) is computed by dividing the absorbed portion of AM1.5 solar irradiation ($I_{\text{AM1.5}}$) by the whole AM1.5 solar irradiation:

$$\bar{\alpha}_{\text{sw}} = \frac{\int_{0.3}^3 \varepsilon(\lambda, \theta_{\text{sun}}) I_{\text{AM1.5}}(\lambda) d\lambda}{\int_{0.3}^3 I_{\text{AM1.5}}(\lambda) d\lambda} \quad (4)$$

A limitation of this work is that it did not account for the reduced long wave radiation trapped by the atmosphere when radiation is emitted from radiative cooling surfaces. However, the implications are expected to be negligible for the large size of the atmosphere when compared to roofs, and for the small emitted radiation flux from cool roofs (their temperature and total emissivity are low)

Table 4
Parameters used for defining air conditioning systems for TEB and BEM [1].

Parameter	Value
Sensible internal heat gains per floor area [W.m^{-2}]	12
Latent internal heat gains per floor area [W.m^{-2}]	1.5
Ventilation rate per floor area [$\text{s}^{-1} \cdot \text{m}^{-2}$]	0.61
Set point temperature for cooling [$^{\circ}\text{C}$]	24
Set point relative humidity [%]	50
Fraction of AC waste heat to the outdoor [%]	60

Table 5
Sensitivity of $\bar{\alpha}_{\text{atm}}$ to day/night effect and to fluctuations in T_{dew} .

Simulation Run	T_{dew} [°C]	$\bar{\alpha}_{\text{atm}}$ Day	$\bar{\alpha}_{\text{atm}}$ Night	$\bar{\alpha}_{\text{atm}}$ Mean	Maximum Deviation from Mean
June 22-24	12 (min)	0.143	0.150	0.152	0.01
	22 (max)	0.154	0.162		
July 12-14	12 (min)	0.143	0.150	0.154	0.011
	25 (max)	0.157	0.165		
August 14-16	14 (min)	0.145	0.153	0.155	0.01
	25 (max)	0.157	0.165		
September 14-16	15 (min)	0.146	0.154	0.155	0.009
	23 (max)	0.155	0.163		

Table 3
Thermo-physical properties used in TEB and BEM Models [1].

Part	Thickness d [m]	Volumetric Heat Capacity C [$\text{MJ m}^{-3} \text{K}^{-1}$]	Thermal Resistance R [$\text{K m}^2 \text{W}^{-1}$]	Albedo of Outer Layer α [-]	Longwave Emissivity of Outer Layer ϵ [-]
Roof	0.16	1.755	0.408	0.225	0.9
Wall	0.54	1.822	0.474	0.5	0.9
Road	1.25	1.509	0.843	0.08	0.95
Inner Floor	0.2	2.016	0.103	-	-

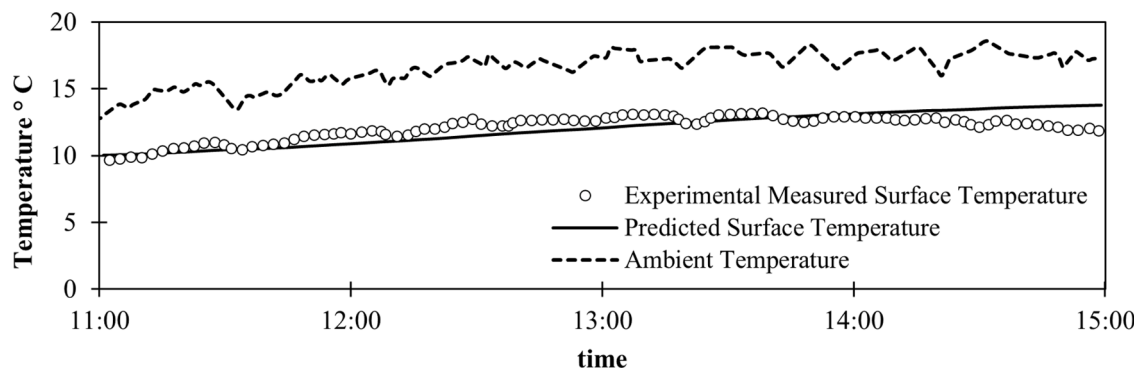
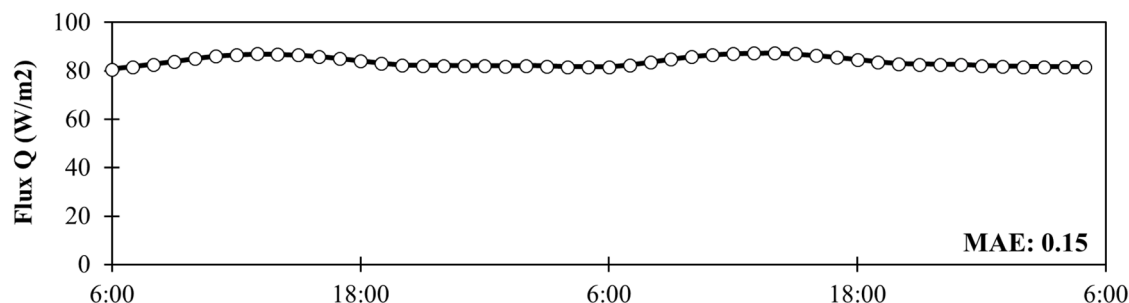


Fig. 5. Validation of the heat transfer model with Raman et al. experiment: Selective radiative cooling material surface temperature predicted and observed in Raman et al. experiment (Raman et al., 2014).

— Emitted flux predicted by TEB
○ Emitted flux predicted using spectral angular RC model

a. Emitted flux predicted by TEB and the spectral directional RC model in July



b. Emitted flux predicted by TEB and the spectral directional RC model in August

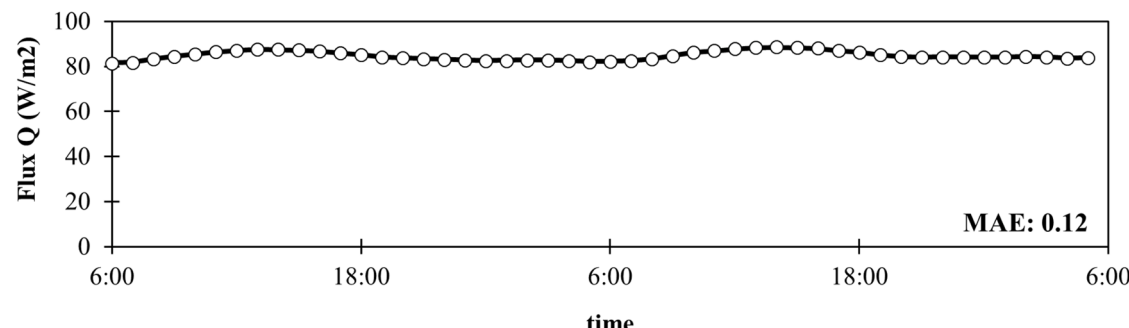


Fig. 6. Predicted emitted longwave fluxes using the spectral angular models and TEB model for a) July and b) August months.

3. Case Study

A case study was conducted to evaluate the impact of RC roof panels on the microclimate of Beirut's city under various humidity levels. The case where the effect of daytime RC layer is considered in the energy balance of the roof is compared to concrete roofs and cool roofs. In the sections that follow, the study domain, inputs for the urban and RC models, effective RC properties calculation, and indicators used for performance assessment are presented.

3.1. Study domain

Beirut (33.89° N, 35.5° E), Lebanon's capital and largest city, has been chosen as the study domain. The Greater Beirut Area (GBA)

encompasses 233.2 km² or 2.2% of Lebanese territory and its land cover is majorly composed of buildings with some vegetation covers (Ghaddar, Ghali, & Ghaddar, 2017). The city is characterized by humid and moderate to hot summers, moderate dry fall and spring, and cold short winters (Lebanon, 2016). Ghaddar et al. investigated the impact of integrating desiccant dehumidification processes to conventional AC systems on UHI in Beirut (Ghaddar et al., 2017). This work implemented the coupling between Meso-NH and TEB atmospheric and microclimate models which was validated through temperature measurements at different locations in the city (Ghaddar et al., 2017). Therefore, their inputs and settings of different models were adopted in the current study.

Three horizontal domains were defined as summarized in Table 1 and shown in Fig. 3. The domains are nested in two ways where the

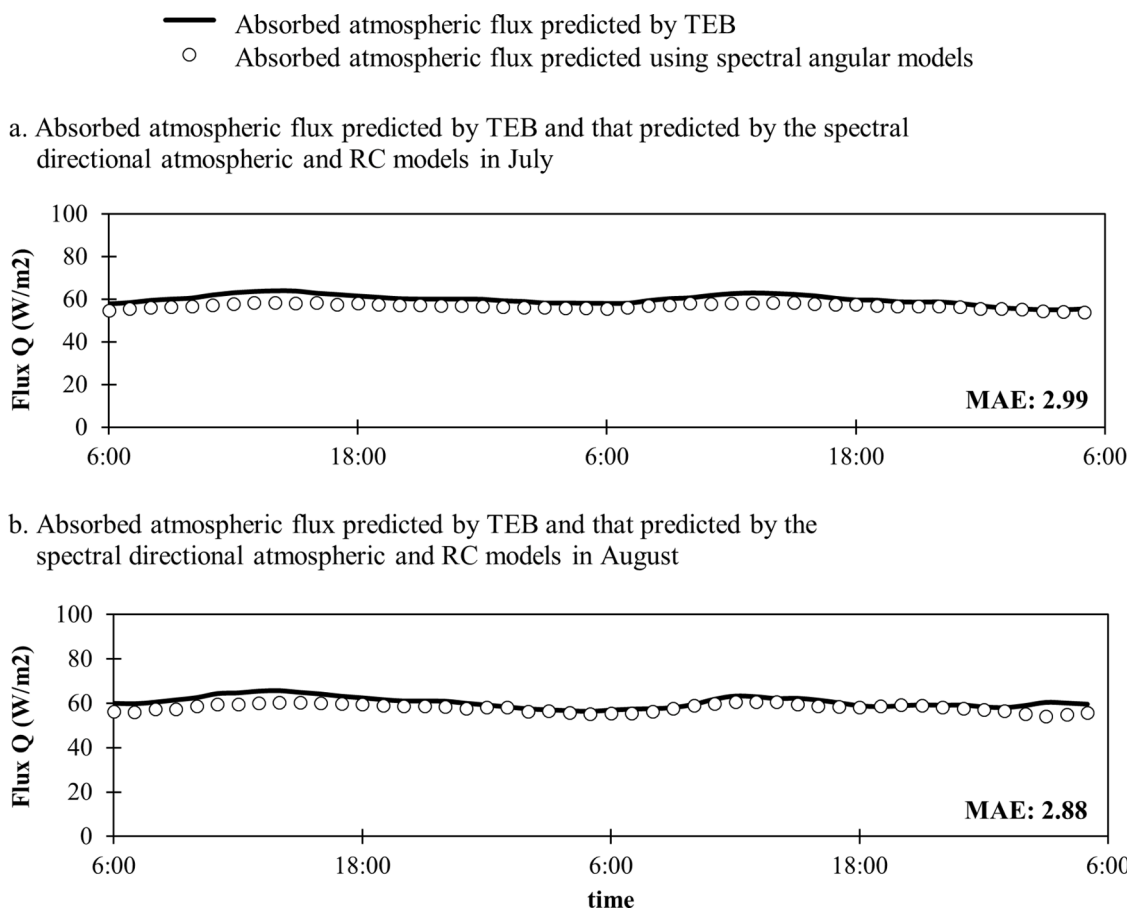


Fig. 7. Atmospheric absorbed flux predicted using the spectral angular models and TEB model for a) July and b) August months.

inner domain influences the outer domain, and the outer domain influences the inner. For the vertical levels, a stretching grid with the highest resolution near the ground at 7 m size is used (see Fig. 3). The maximum allowed difference between vertical levels is set to 400 m while ensuring that the upper part of the grid is in the stratosphere region such that the assumption of free slip upper boundary condition is valid for the atmospheric model (P. Bechtold, 2014).

3.2. Input parameters of the urban microclimate model

The initial conditions for all domains and the boundary conditions for the outer domain were obtained using the fifth generation of the atmospheric re-analysis for the global climate (ERA5) from the European Centre for Medium-Range Weather Forecasts (ECMWF). ERA5 has a 30 km spatial resolution compared to ~80 km resolution of its predecessor, ERA-Interim (ECMWF). The simulation time was set to 48 hours starting at 6:00 a.m. on each of June 22, July 12, August 14, and September 14, 2021. The chosen days have different humidity levels, which allows assessing the humidity effect on RC performance. Since numerical weather models require time to reach their own climatology to achieve a physically valid state (known as “spin-up time”) (Ulmer & Balss, 2016), each simulation was run for 24 hours prior to the actual start time. Surface elevation above sea level and surface cover were defined using NASA’s Shuttle Radar Topography Mission SRTM (see Fig. 4 (b)) (Farr et al., 2007) and ECOCLIMAP (Champeaux, Masson, & Chauvin, 2005) databases, respectively. Table 2 outlines the data sources utilized in the simulation.

TEB and BEM inputs were obtained from a variety of sources. The building density was calculated using ArcGIS Pro software using a GIS shape file of buildings in the city (see Fig. 4 (a)). As for the buildings’

heights, the reported values by Krayem et al. were used (Krayem, Yeretzian, Faour, & Najem, 2021). Then, the wall to urban area ratio was estimated using the heights and perimeters of buildings while the aerodynamic roughness length was estimated to be one tenth of the building height based on literature (Burian, Velugubantla, & Brown, 2002; Grimmond & Oke, 1999). The thermal roughness length was determined using the Kanda-2007 scheme, which is based on experimental data from the Comprehensive Outdoor Scale Model (COSMO) (Kanda, Kanega, Kawai, Moriawaki, & Sugawara, 2007). Facade glazing ratio of buildings was set to 0.3, the Solar Heat Gain Coefficient of windows (SHGC) was set to 0.8 and their U-factor was set to 5.8 m²/K based on data from a survey conducted in Beirut and on Thermal Standard for Buildings in Lebanon (TSBL) (Annan, Ghaddar, & Ghali, 2016; OEA, 2010). The thermal conductivity, specific heat, and thickness of walls, roofs, and roads layers as well as the cooling systems parameters were adopted from Ghaddar et al. (Ghaddar et al., 2017). The shortwave reflectivity and the emissivity for concrete roofs were set to 0.225 (Kaloustian, Bitar, & Diab, 2016) and 0.9 (Ghaddar et al., 2017) respectively. The thermos-physical characteristics for buildings and roads are summarized in Table 3.

Finally, the anthropogenic heat from the transportation sector was estimated by Sailor’s approach (Sailor & Lu, 2004) with data for Beirut city including the population and area of Beirut (UN, 2020), the per capita ownership of personal vehicles, the transport energy intensity, the average velocity and trip distance (MoE, 2012), and the estimated delay per trip during peak hours (Saroufim & Otayek, 2019). Assuming the latent portion of traffic anthropogenic heat to be 8% (Pigeon, Legain, Durand, & Masson, 2007), sensible and latent anthropogenic heat releases were weighted by the fraction of roads in the city. In average, sensible and latent fluxes from transportation in urban areas were 10.8

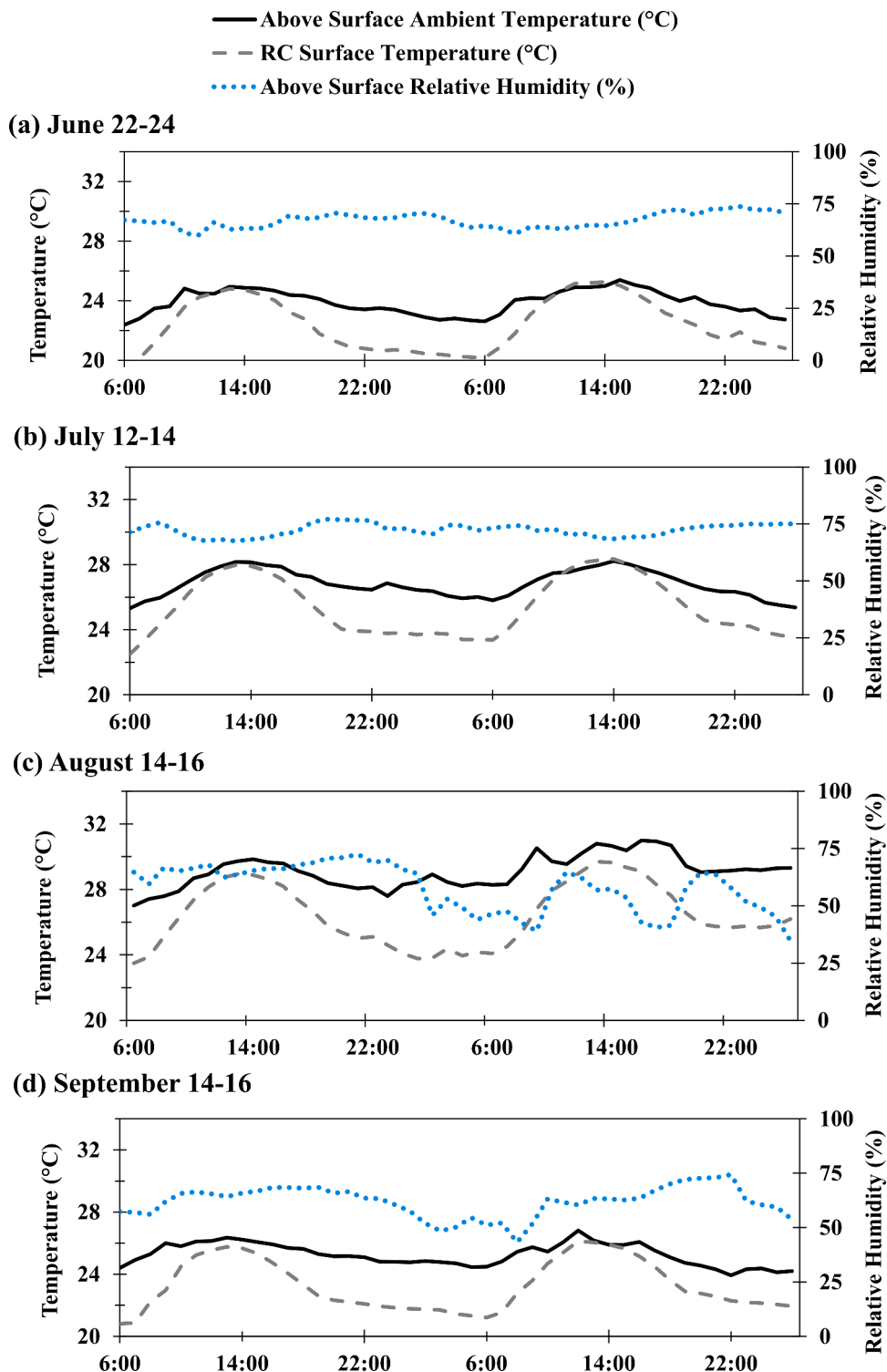


Fig. 8. RC surface temperature compared to above surface ambient air temperature at Location 1 (Mid-building density) for simulation days having different air humidity levels: (a) June 22 to 24 (b) July 12 to 14 (c) August 14 to 16 and (d) September 14 to 16.

W/m^2 and 0.94 W/m^2 , respectively. Because industries are few in Beirut (Ghaddar et al., 2017) no particular treatment for industrial fluxes was undertaken, and the default uniform value in TEB of 5 W/m^2 was kept. Human metabolism outside of buildings was relatively negligible and ignored. However, BEM accounts for metabolism inside buildings (Moigne, 2012). Table 4 outlines the characteristics used to define the air conditioning systems of buildings in the city.

3.3. Radiative properties for RC and reflective roofs' layers

In this work, the properties of Raman et al. daytime RC material are used (Raman et al., 2014). The photonic radiative cooler consists of seven alternating layers of silicon dioxide (SiO_2) and hafnium dioxide (HfO_2) of varying thicknesses, on top of 200 nm of silver (Ag), which are all deposited on top of a 200-mm silicon wafer. The material can reflect 97% of solar radiation while emitting powerfully and selectively in the

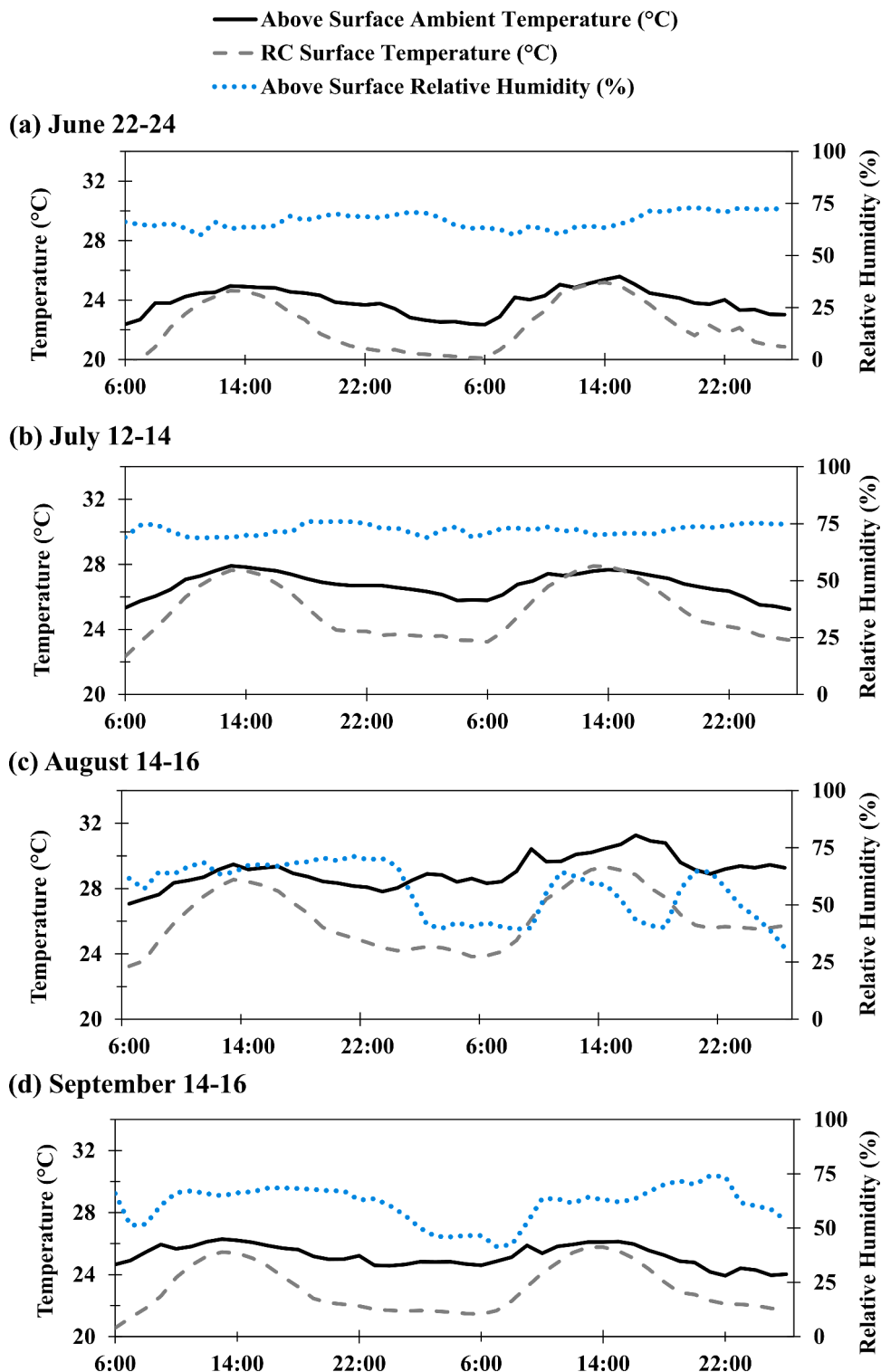


Fig. 9. RC surface temperature compared to above surface ambient air temperature at Location-2 (High building density) for simulation days having different air humidity levels: (a) June 22 to 24 (b) July 12 to 14 (c) August 14 to 16 and (d) September 14 to 16.

atmospheric transparency window (Raman et al., 2014). The combined effect of high shortwave reflectance and selective emissivity allows the material to maintain a sub-ambient surface temperature even under direct sunlight exposure.

The angular spectral emissivity of the material was obtained by William Paterson University's tool for Thermal Energy and Radiation management with multi-layer nanostructures (WPThermI) (Varner, Eldabagh, Volta, Eldabagh, & Foley, 2019). Cool roofs were

implemented by adding a roof layer with an albedo value of 0.88, which is the value of EPA Energy Star SOLARFLECT coating (Li & Norford, 2016). The albedo of the cool roofs degrades with time; nonetheless, it is aimed to compare the impact of RC panels to the upper limit of impact of cool roofs, to avoid any results biasing towards the RC panels. As a result, the albedo of a non-degraded highly performing coating was implemented for comparison.

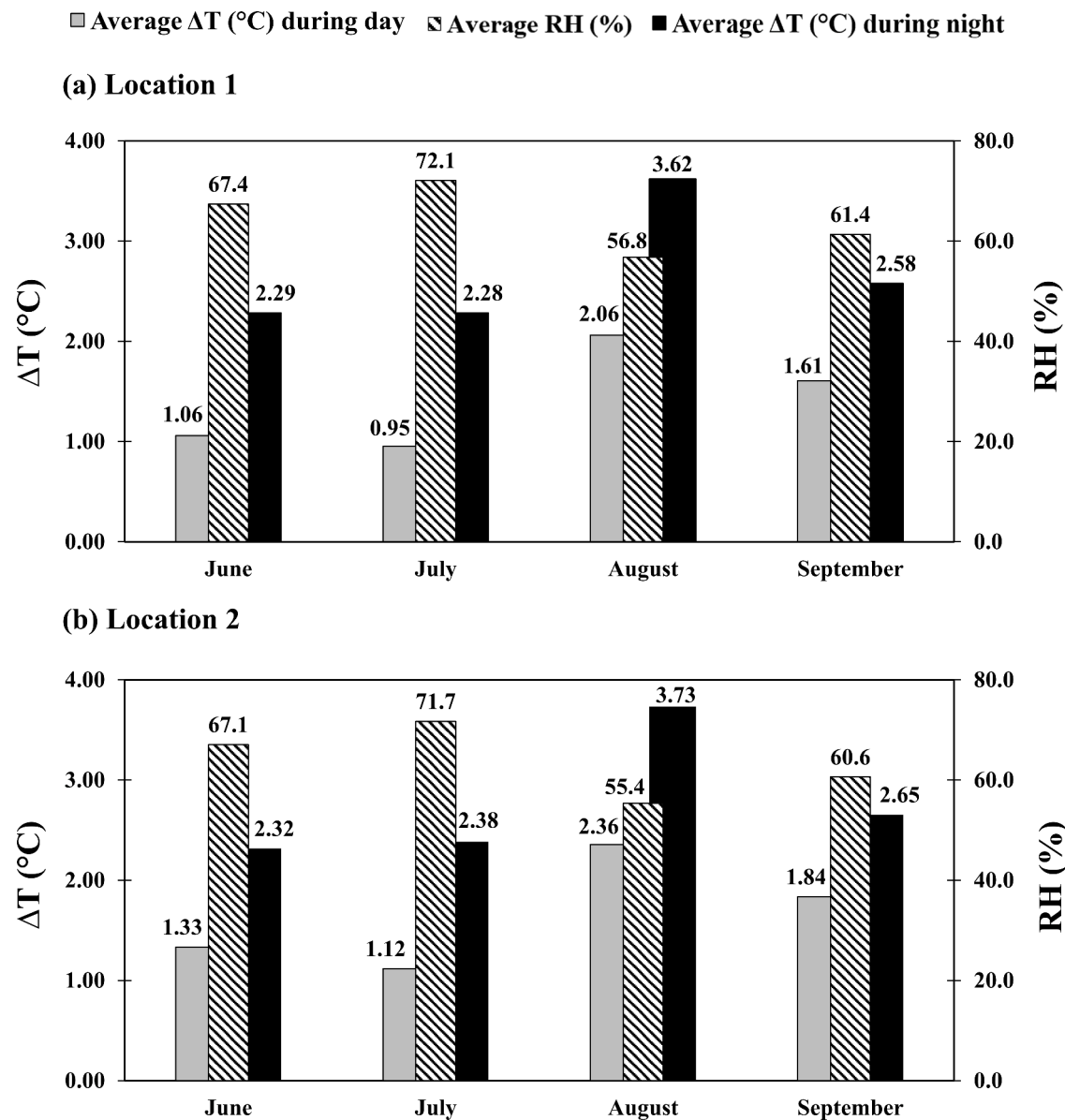


Fig. 10. Average difference between ambient and RC surface temperatures and average relative humidity for simulated days in different months (a) at Location 1 (Mid-building density) and (b) at Location 2 (High-building density).

3.4. Determination of effective RC properties

The effective emissivity $\bar{\varepsilon}$ is calculated using equation (2) while considering the spectral angular emissivity $\varepsilon(\lambda, \theta)$ of Raman's RC material. The atmospheric emissivity ε_{atm} depends on T_{dew} and varies between day and night. This might cause variations in the implemented effective atmospheric absorptivity value $\bar{\alpha}_{atm}$. The mean value of $\bar{\alpha}_{atm}$ for each simulation run is used. The range of T_{dew} encountered at each simulation run is obtained from multiple T_{dew} sensors located at the domain of simulation given by Weather Underground (WU) website (TWC, 2021). Table 5 shows the computed $\bar{\alpha}_{atm}$ for the highest and lowest T_{dew} at day and night for each simulation run as well as $\bar{\alpha}_{atm}$ mean and the maximum possible deviation from mean. The maximum deviation from $\bar{\alpha}_{atm}$ mean due to T_{dew} fluctuations and to day/night effect was 0.011 for all simulation runs (see Table 5).

Finally, $\bar{\alpha}_{sw}$ was calculated using equation (4) while considering $\varepsilon(\lambda, \theta)$ of the studied RC material in the shortwave range and AM (1.5) obtained by the Simple Model of the Atmospheric Radiative Transfer of Sunshine SMARTS (Gueymard, 2009). The effective hemispherical

shortwave absorptivity $\bar{\alpha}_{sw}$ was found to be around 0.03, which is consistent with what has been reported by Raman et al. (Raman et al., 2014).

3.5. Indicators for performance

The impact of RC panels was studied in comparison to a baseline case in which the roofs are made of concrete. Moreover, the performance was compared to that of cool roofs as a traditional UHI mitigation measure. Two indicators of performance were used as follows:

- i) The drop in air temperature at pedestrian level, ΔT_{air} which was assessed first throughout the city during peak hours, then in selected locations with respect to time.
- ii) The drop in the Universal Thermal Climate Index ($\Delta UTCI$), which was used to assess the impact of RC on outdoor thermal comfort at street level. $UTCI$ is defined as the equivalent temperature at certain reference conditions that produces the same response predicted by a bioheat model as actual conditions. It is applicable in a wide range of

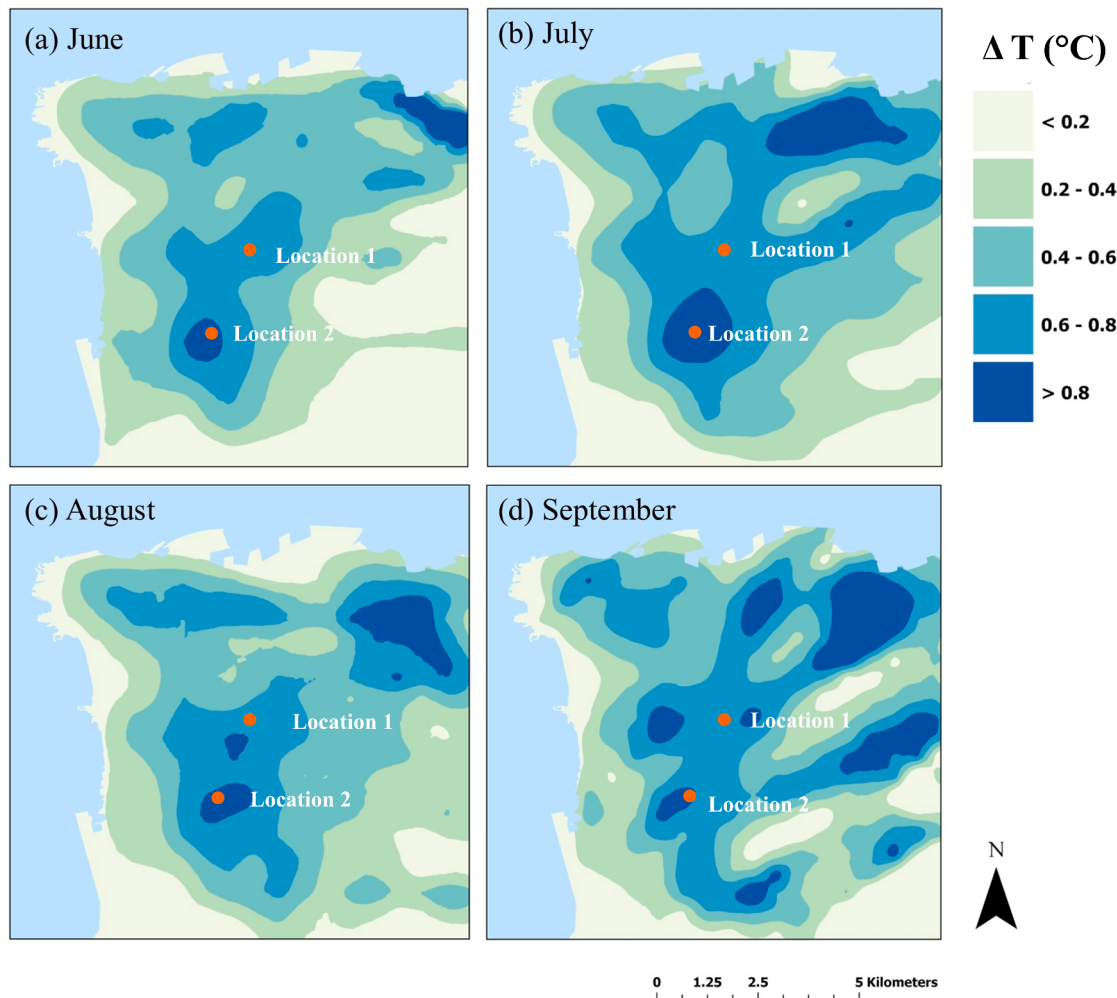


Fig. 11. Decrease in T_{air} due to considering the effect of daytime RC panels on the energy balance of roofs in the city of Beirut at 14:00 on (a) June 23, 2021; (b) July 13, 2021; (c) August 15, 2021; and (d) September 15, 2021.

climates, and it is calculated by TEB using the Brode et al. equation (Bröde et al., 2012). Because the thermal environment in the study domain is expected to cause heat stress, the effectiveness of RC was measured in terms of UTCI reduction to reflect improved thermal comfort.

4. Validation of Simulation Results

The coupled models: Meso-NH, Town Energy Balance TEB, and its building energy model BEM have been used and experimentally validated in a previous work for Beirut city (Ghaddar et al., 2017). The baseline simulation with concrete roofs employed the same settings defined by the reference (Ghaddar et al., 2017), including buildings thermos-physical characteristics and air conditioning system parameters. The results of Ghaddar et al. were regenerated to ensure that the models produce the same output.

4.1. Validation of the spectral angular atmospheric and RC models

The integration between the spectral angular RC model and the spectral angular atmospheric models used to calculate effective properties was validated by comparing the transient surface temperature predicted by the models with that observed in an experiment done by Raman et al. at Stanford, California in mid-December 2013 (Raman et al., 2014). The following input parameters were used: solar incident radiation, ambient air temperature, ambient air dew point, and

convective-conductive losses. The authors of the referred study provided all inputs except the dew temperature of the ambient air. We used the average dew temperature of days from December 13 to December 17, 2013, recorded by Norman Y. Mineta San Jose International Airport weather station. The surface temperature predicted by the model correlates with the temperature measured experimentally, as shown in Fig. 5.

4.2. Validation of implementation of selective RC materials in TEB-BEM

In this work, spectral angular models for the atmosphere and the RC materials were used to obtain the portion of atmospheric incident radiation absorbed by the RC surface, the portion of radiation emitted from surface compared to blackbody and the portion of solar incident radiation absorbed by the surface, then implement them into urban simulation models. The implementation was done by altering the energy balance of buildings' roofs in the town. The integration technique was validated by comparing the radiative fluxes predicted by TEB using the effective properties approach to those predicted by the validated spectral angular models.

The ambient air temperature and dew point and the surface temperature were extracted from TEB and used as inputs to the spectral angular models. The spectral emitted radiation was calculated by the spectral model and then integrated over the longwave wavelength range to obtain the emitted flux. The values predicted by the two models agreed well with each other at mean absolute error (MAE) of 0.12-

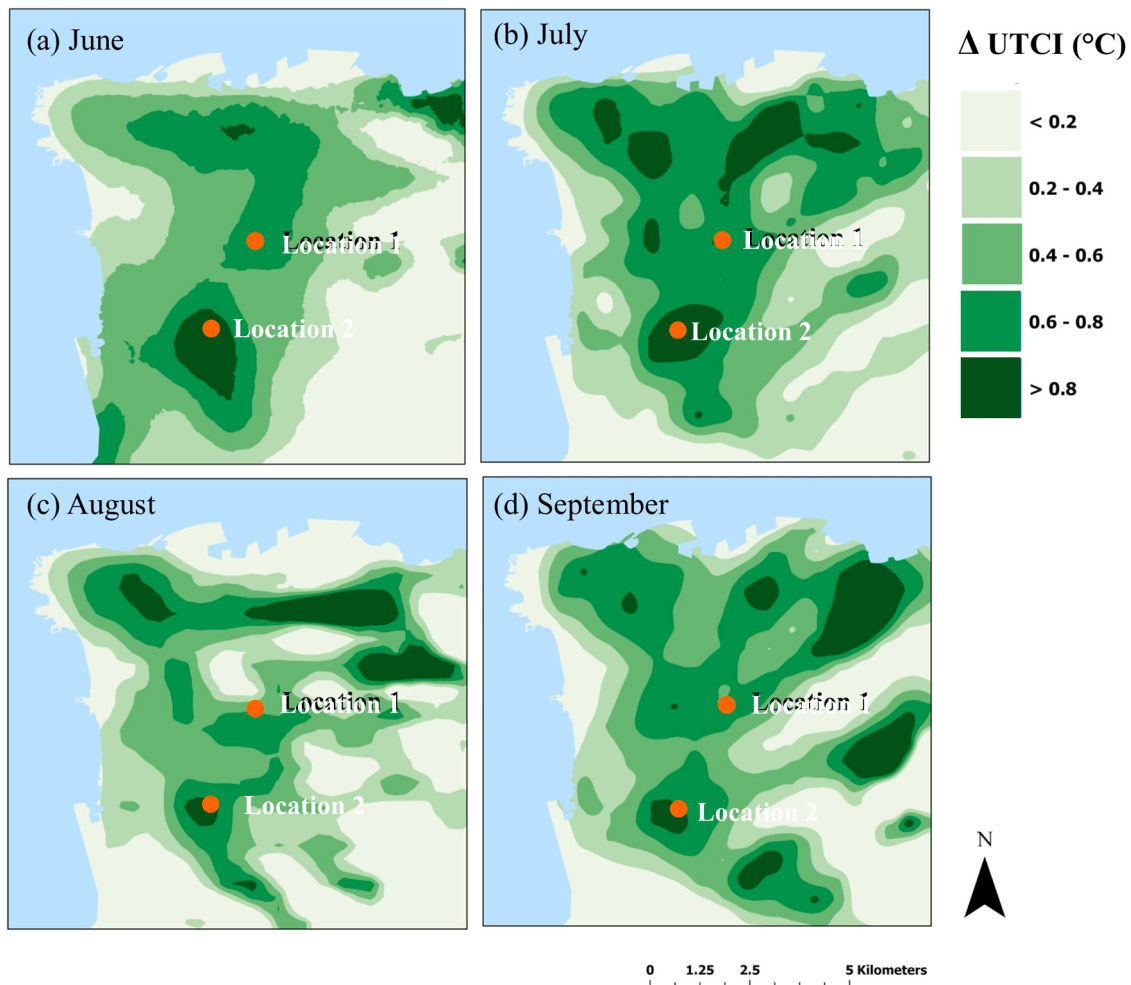


Fig. 12. Decrease in UTCI due to considering the effect of daytime RC panels on the energy balance of roofs in the city of Beirut at 14:00 on (a) June 23, 2021; (b) July 13, 2021; (c) August 15, 2021; and (d) September 15, 2021.

0.15W/m² as shown in Fig. 6(a) for July and Fig. 6(b) for August.

The ambient temperature and dew point are used as inputs for Berger atmospheric model and Granqvist's equation to obtain the spectral angular radiation emitted from atmosphere. By integrating over the longwave range, the absorbed atmospheric radiation was obtained and compared to that predicted by TEB model. The values predicted by the two models agreed well with each other for the two test months as shown in Fig. 7(a) and Fig. 7(b). The mean absolute difference was 2.88–2.99 W/m²

5. Results and Discussion

In this section, the predicted surface temperature of the RC panels is presented and compared to the ambient air temperature in four months with varying humidity levels. The impact of RC roof panels on Beirut's microclimate is then investigated and compared to that of cool roofs using the established performance metrics ΔT_{air} and $\Delta UTCI$. Finally, additional analysis is performed in terms of radiative fluxes and surface temperature for concrete roofs, cool roofs, and RC panels. "Location 1" (33.865° N, 35.518° E) in a medium building density region (0.3–0.4) and "Location 2" (33.847° N, 35.513° E) at a high building density region (0.4) were chosen as representative locations for results presentation.

5.1. RC panels surface temperature under different meteorological conditions

Fig. 8 and Fig. 9 show the surface temperature of RC panels as well as the ambient above-surface temperature and relative humidity (RH) for simulated days in (a) June, (b) July, (c) August, and (d) September at locations 1 and 2, respectively. It is clear that the RC panels can maintain sub-ambient temperatures during most hours of the day for all summer months. Nonetheless, the difference between surface and ambient temperatures was higher at night and minor during peak day hours due to the influence of solar radiation. Simulated days in July with the highest air humidity ($\bar{RH} \sim 72\%$) had a maximum surface-ambient ΔT of around 3°C at night (23:00) and a minimum ΔT of around -0.3°C at peak temperature hour (13:00). Whereas in August which had the lowest air humidity ($\bar{RH} \sim 56\%$), the ambient-surface ΔT reached a maximum of around 5°C at night (2:00) and a minimum of around 1°C at peak temperature hour (13:00). The average ambient-surface ΔT during day and night and the average relative humidity above surface for simulated days of each month are presented in Fig. 10. The average ΔT in July (High RH) was around 1°C during day and around 2.3°C during night compared to ΔT in August (Mid RH) which was around 2.3°C during daytime and around 3.65°C during night. The temperature difference (ΔT) between the RC surface and the ambient was larger during months with lower humidity, indicating better RC performance. In the upcoming analysis, simulation days in July and August are chosen to represent high and mid humidity conditions, respectively.

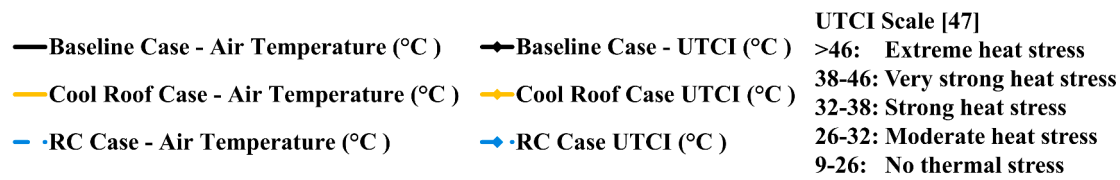
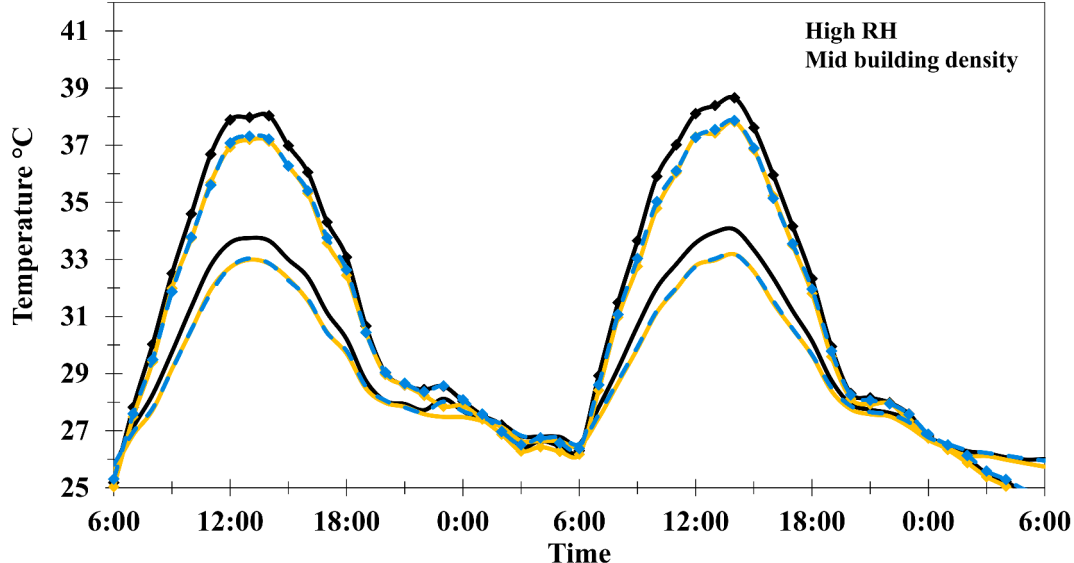
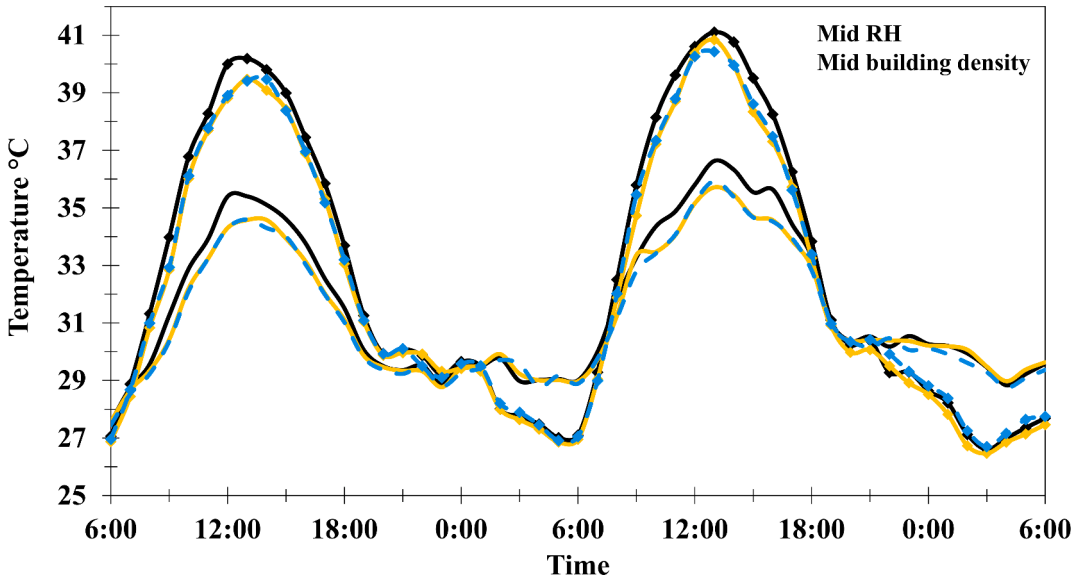
(a) T_{air} and UTCI from July 12 to July 14, 2021 at Location 1(b) T_{air} and UTCI from August 14 to August 16, 2021 at Location 1

Fig. 13. Pedestrian level (2m) T_{air} ($^{\circ}\text{C}$) and UTCI ($^{\circ}\text{C}$) at Location 1 (Mid-building density) corresponding to concrete roof (black), cool roof (yellow), and RC roof panels (blue) (a) for days in July (High RH) and (b) for days in August (Mid-RH).

5.2. Impact of RC roof panels on pedestrian level air temperature and thermal comfort

Fig. 11 shows the area map of the drop in air temperature at pedestrian level (2m), ΔT_{air} , due to the RC roof compared to concrete roof at 14:00 on (a) June 23, 2021; (b) July 13, 2021; (c) August 15, 2021; and (d) September 15, 2021. It was observed that the RC roof panels reduced the air temperature in a similar manner throughout simulated days of the four months. The air temperature at pedestrian

level in most of the domain was decreased by at least 0.4°C . The greatest temperature drop occurred in the high building density areas, as contrasted in Fig. 4 (a), where such areas experienced a temperature drop of more than 0.8°C . The drop in total anthropogenic heat released in such areas would be larger as they have higher roof-coverage area, resulting thereby in a pronounced air temperature drop compared to low-density areas. The UTCI drop for a person standing in the shadow at street level ΔUTCI is depicted in Fig. 12 as an area map. The drop of UTCI reflects enhanced outdoors thermal comfort in the studied heat stressful environment.

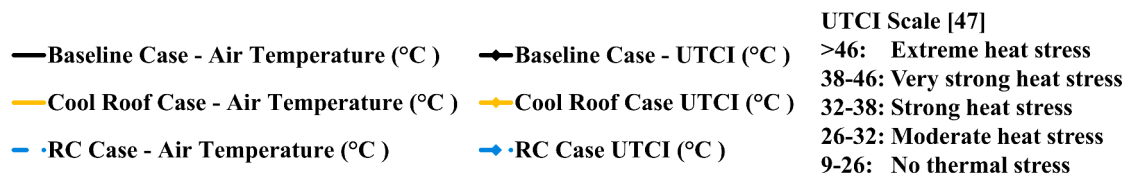
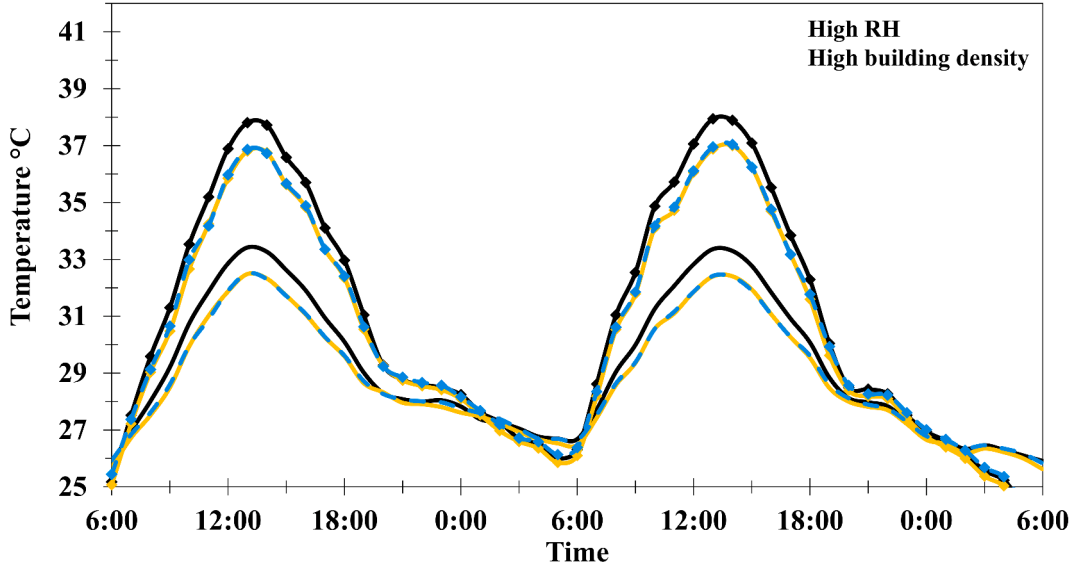
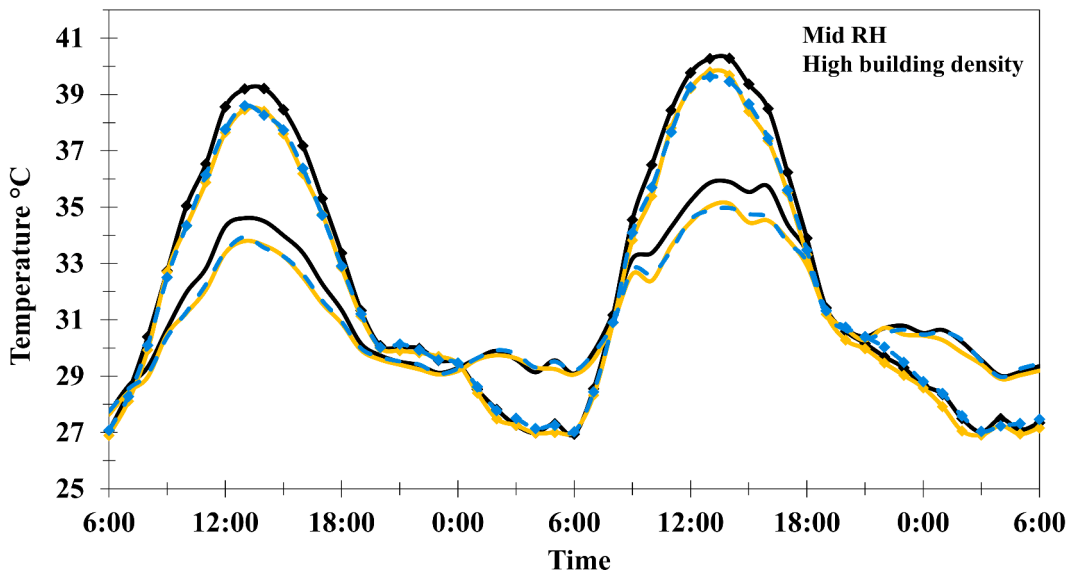
(a) T_{air} and UTCI from July 12 to July 14, 2021 at Location 2(b) T_{air} and UTCI from August 14 to August 16, 2021 at Location 2

Fig. 14. Pedestrian level (2m) T_{air} (°C) and UTCI (°C) at Location 2 (High building density) corresponding to concrete roof (black), cool roof (yellow), and RC roof panels (blue) (a) for days in July (High RH) and (b) for days in August (Mid-RH).

The primary cause of the decrease in UTCI was the drop in air temperature which explains the similarity in the area maps of Δ UTCI to the area maps of ΔT .

Air temperature at pedestrian level (T_{air}) and UTCI corresponding to the cases of concrete roofs, cool roofs, and RC panels are plotted against time at Location 1 (Mid building density), for days in July (High RH) and August (Mid-RH) in Fig. 13(a) and Fig. 13(b), respectively and at Location 2 (High building density) for days in July and August in Fig. 14(a) and Fig. 14(b), respectively. One can draw four main observations

from the figures: i) similar drop in T_{air} and UTCI due to RC panels was experienced in high and medium humidity months, which reflect, the RC panels' impact on the microclimate was not significantly enhanced in lower humidity conditions; ii) the significant microclimate impact of RC panels occurred only during the day, despite that they caused a greater surface ambient ΔT at night; iii) RC panels had a similar impact to high performance cool roofs in the two months (mid and high RH), at the two locations (mid and high building density), with both causing a comparable drop in T_{air} and UTCI during simulation time; and iv) the impact of

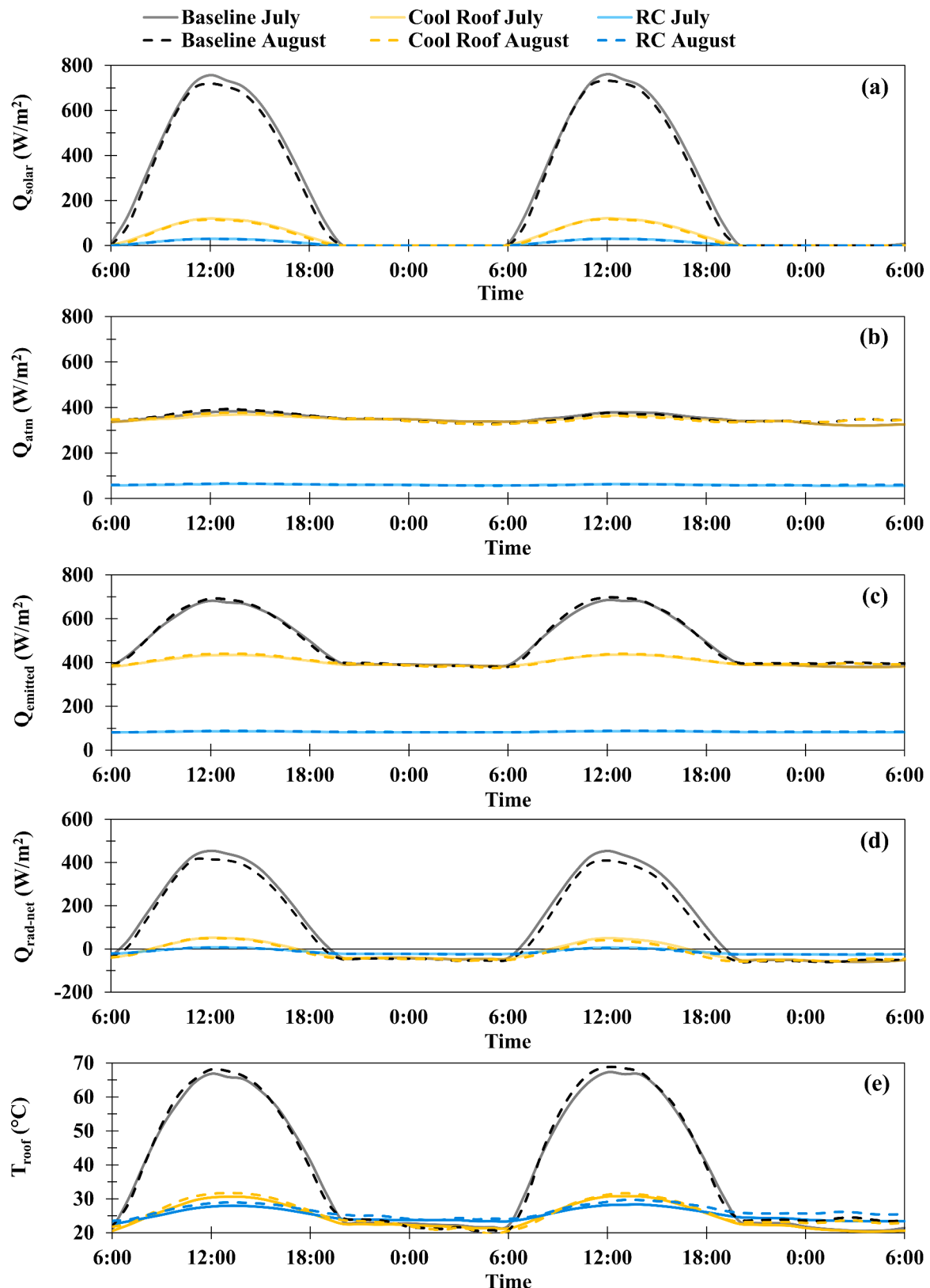


Fig. 15. Comparison between concrete, cool roof, and RC roofs for days in July (High RH) and August (Low RH) at Location 1 (Mid-building density) in terms of (a) Absorbed solar flux Q_{solar} (W/m^2) (b) Absorbed atmospheric flux Q_{atm} (W/m^2) (c) Emitted flux Q_{emitted} (W/m^2) (d) Net radiative flux $Q_{\text{rad}-\text{net}}$ (W/m^2) and (e) Roof temperature T_{roof} ($^{\circ}\text{C}$).

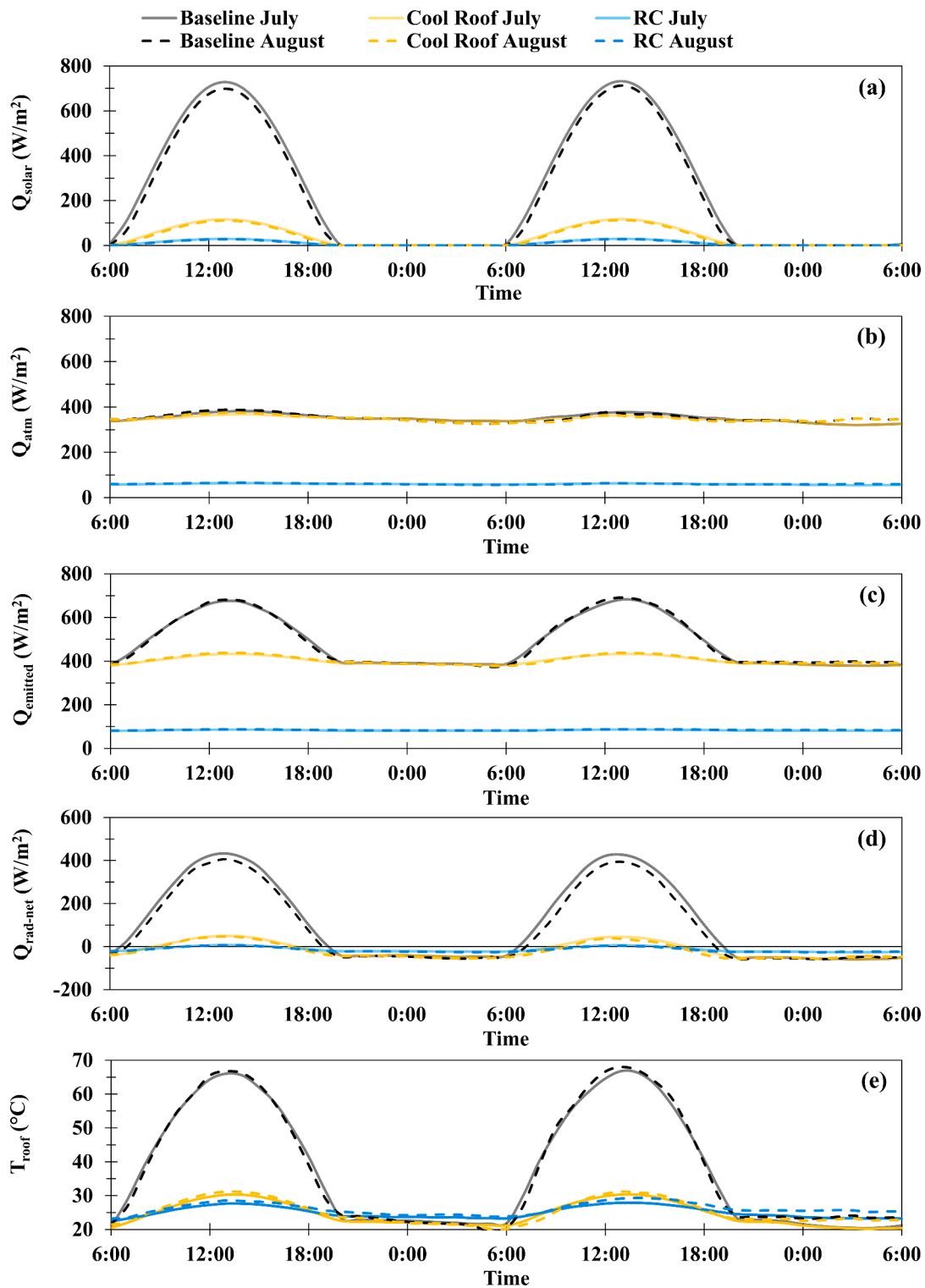


Fig. 16. Comparison between concrete, cool roof, and RC roofs for days in July (High RH) and August (Low RH) at Location 2 (High-building density) in terms of (a) Absorbed solar flux Q_{solar} (W/m^2) (b) Absorbed atmospheric flux Q_{atm} (W/m^2) (c) Emitted flux Q_{emitted} (W/m^2) (d) Net radiative flux $Q_{\text{rad}-\text{net}}$ (W/m^2) and (e) Roof temperature T_{roof} ($^{\circ}\text{C}$).

both RC panels and cool roofs was greater in higher building density location.

More in depth analysis is needed to determine why RC panels and cool roofs performed similarly, and why RC panels' impact on T_{air} and UTCI was not significantly improved in lower humidity settings. In the following subsection, the radiative fluxes of [Equation \(1\)](#) are presented for the different roof scenarios, in high and mid-humidity settings at

high and mid-building density locations for further analysis.

5.3. Radiative fluxes and surface temperature analysis

The analysis of radiative fluxes helps in understanding the independent influence of reflectance and selective emissivity of daytime RC materials. [Figs. 15\(a\)](#) and [16\(a\)](#) show the absorbed solar flux Q_{solar} by

the upper roof layer during the months of July and August at Location 1 and Location 2, respectively. Both cool roofs and RC layers were found to reduce Q_{solar} significantly, with the RC layer yielding the largest reduction.

Figs. 15(b) and 16(b) show the absorbed atmospheric flux Q_{atm} for the upper roof layer in July and August months at Location 1 and Location 2, respectively. The selective properties of the RC layer caused a large drop in Q_{atm} when compared to the concrete and cool roofs. Radiation emitted from atmosphere is dependent on both ambient air temperature and air humidity. Although August had higher ambient air temperature than July, Q_{atm} absorbed by the RC panel was comparable in the two months. This is explained by the reduction of ϵ_{atm} due to lower ambient air humidity in August.

Figs. 15(c) and 16(c) shows the emitted longwave flux for different roof cases in July and August at Location 1 and Location 2, respectively. The difference in surface temperature and in total emissivity of different roof layers can explain the difference in Q_{emitted} . The concrete roof emitted the most energy flux, followed by the reflective roof, and lastly the RC roof which had the minimum emitted flux. This indicates that the selective spectral RC characteristics -that resulted in a drop in atmospheric absorbed radiation- have also yielded a drop in total emitted radiation.

The net radiative flux $Q_{\text{rad-net}}$ is presented for the three roof cases in Figs. 15(d) and 16(d) at Location 1 and Location 2, respectively. In the RC case, $Q_{\text{rad-net}}$ was negative except during peak day hours, where the hot humid climate of Beirut caused a small positive net which was smaller in August. Cool roofs, on the other hand, exhibited a positive during the day but a negative net at night. $Q_{\text{rad-net}}$ of cool roofs was lower than that of RC panels during night due to the larger emitted flux.

Finally, in Figs. 15(e) for Location 1 and 16(e) for Location 2, the surface temperature of all concrete, cool roofs, and RC panels throughout simulation days in the two months is presented. Only RC panels achieved sub-ambient temperatures during the day, but both RC and cool roofs significantly reduced surface temperature. The major impact of RC and reflective layers on the surface temperature of the roof occurred during the day, resulting in a significant reduction in cooling load and associated anthropogenic heat during that period.

Fig. 16.

In summary, the high shortwave reflectivity of daytime RC panels and cool roofs resulted in a significant reduction in absorbed solar energy. The selective RC characteristics lowered the absorbed air radiation, but they also reduced the overall emitted radiation. The surface temperature of the RC and cool roofs was much lower than that of concrete roofs, with the RC panels slightly cooler than the cool roofs. The small difference between RC and cool roof in terms of surface temperatures did not yield in a significant difference in terms of the impact on waste heat reduction and pedestrian T_{air} . These findings explain why RC and cool roofs had a comparable effect on pedestrian T_{air} and why their impact was limited to daytime.

6. Conclusion

Waste heat from building cooling systems contributes to the intensification of the urban heat island effect. Installing RC panels reduces cooling loads in buildings, resulting in less heat being emitted into the microclimate. The effective radiative properties of RC panels were determined in this study using their spectral angular properties and a spectral angular atmospheric model, and the effect of installing RC roof panels on microclimate air temperature and outdoor thermal comfort was evaluated using coupled atmospheric, microclimate, and building energy models for Beirut as a case study. The effectiveness of the RC device was evaluated in comparison to roofs made of typical building materials. Furthermore, the performance of RC panels was compared to that of cool roofs, which are commonly used in cities to mitigate UHI. The results can be summarized as follows:

- In terms of surface temperature, daytime RC panels outperformed high performance high performance cool roofs, but in terms of anthropogenic heat reduction and microclimate air temperature reduction, they both had a similar impact.
- In Beirut hot humid conditions, the performance of daytime RC panels was better in low humidity conditions when assessed using surface temperature, but the effect of RC panels on microclimate was similar in simulated days with high and mid humidity.
- The surface temperature of daytime RC panels dropped more during the night, but due to the significant reduction in surface temperature during the day when compared to concrete roofs, the effect on microclimate air temperature and thermal comfort was limited to daytime.
- The impact of RC panels was higher in regions with higher building density. Such areas experienced a larger drop in pedestrian air temperature and corresponding UTCI thermal comfort index.

In conclusion, in the hot humid weather of Beirut, RC roof panels had a comparable impact on UHI effect to high performance cool roofs.

Declaration of Competing Interest

None.

References

- Akbari, H., & Konopacki, S. (2004). Energy effects of heat-island reduction strategies in Toronto, Canada. *Energy*, 29(2), 191–210.
- Annan, G., Ghaddar, N., & Ghali, K. (2016). Natural ventilation in Beirut residential buildings for extended comfort hours. *International Journal of Sustainable Energy*, 35 (10), 996–1013.
- Berger, X., & Bathiebo, J. (1989). From spectral clear sky emissivity to total clear sky emissivity. *Solar & wind technology*, 6(5), 551–556.
- Bonafoni, S., Baldinelli, G., & Verducci, P. (2017). Sustainable strategies for smart cities: Analysis of the town development effect on surface urban heat island through remote sensing methodologies. *Sustainable cities and society*, 29, 211–218.
- Bröde, P., Fiala, D., Blażejczyk, K., Holmér, I., Jendritzky, G., Kampmann, B., ... Havenith, G. (2012). Deriving the operational procedure for the Universal Thermal Climate Index (UTCI). *International journal of biometeorology*, 56(3), 481–494.
- Burian, S. J., Velugabantla, S. P., & Brown, M. J. (2002). Morphological analyses using 3D building databases: Phoenix, Arizona. *Los Alamos National Laboratory*.
- Carlosena, L., Ruiz-Pardo, Á., Feng, J., Irulegi, O., Hernández-Minguillón, R. J., & Santamouris, M. (2020). On the energy potential of daytime radiative cooling for urban heat island mitigation. *Solar Energy*, 208, 430–444.
- Coutts, A. M., Daly, E., Beringer, J., & Tapper, N. J. (2013). Assessing practical measures to reduce urban heat: Green and cool roofs. *Building and Environment*, 70, 266–276.
- ECMWF. Fifth generation of ECMWF atmospheric reanalyses of the global climate. Retrieved from <https://cds.climate.copernicus.eu/cdsapp#!/home> (retrieved on September 1, 2021).
- Feng, J., Khan, A., Doan, Q.-V., Gao, K., & Santamouris, M. (2021). The heat mitigation potential and climatic impact of super-cool broadband radiative coolers on a city scale. *Cell Reports Physical Science*, 2(7), Article 100485.
- Gentle, A., Aguilar, J., & Smith, G. (2011). Optimized cool roofs: Integrating albedo and thermal emittance with R-value. *Solar Energy Materials and Solar Cells*, 95(12), 3207–3215.
- Ghaddar, Z., Ghali, K., & Ghaddar, N. (2017). Impact of integrating desiccant dehumidification processes to conventional AC system on urban microclimate and energy use in Beirut city. *Energy Conversion and Management*, 153, 374–390.
- Ghali, K., Ghaddar, N., & Bizri, M. (2011). The influence of wind on outdoor thermal comfort in the city of Beirut: a theoretical and field study. *HVAC&R Research*, 17(5), 813–828.
- Granqvist, C., & Hjortsberg, A. (1981). Radiative cooling to low temperatures: General considerations and application to selectively emitting SiO films. *Journal of Applied Physics*, 52(6), 4205–4220.
- Grimmond, C., & Oke, T. R. (1999). Aerodynamic properties of urban areas derived from analysis of surface form. *Journal of Applied Meteorology and Climatology*, 38(9), 1262–1292.
- Gueymard, C. (2009). Simple model of the atmospheric radiative transfer of sunshine (SMARTS). *Algorithms and performance assessment*.
- Guo, A., Yang, J., Xiao, X., Xia, J., Jin, C., & Li, X. (2020). Influences of urban spatial form on urban heat island effects at the community level in China. *Sustainable cities and society*, 53, Article 101972.
- Ishii, T., Tsujimoto, M., Yoon, G., & Okumiya, M. (2009). Cooling system with water mist sprayers for mitigation of heat-island. In *Paper presented at the Proceedings of the Seventh International Conference on Urban Climate*.
- Kaloustian, N., Bitar, H., & Diab, Y. (2016). Urban heat island and urban planning in Beirut. *Procedia engineering*, 169, 72–79.

- Kanda, M., Kanega, M., Kawai, T., Moriwaki, R., & Sugawara, H. (2007). Roughness lengths for momentum and heat derived from outdoor urban scale models. *Journal of Applied Meteorology and Climatology*, 46(7), 1067–1079.
- Kirchhoff, G. (1978). Über das Verhältnis zwischen dem Emissionsvermögen und dem Absorptionsvermögen der Körper für Wärme und Licht. In. *Von Kirchhoff bis Planck* (pp. 131–151). Springer.
- Kolokotsa, D., Santamouris, M., & Zerefos, S. (2013). Green and cool roofs' urban heat island mitigation potential in European climates for office buildings under free floating conditions. *Solar Energy*, 95, 118–130.
- Krayem, A., Yeretzian, A., Faour, G., & Najem, S. (2021). Machine learning for buildings' characterization and power-law recovery of urban metrics. *PLoS one*, 16(1), Article e0246096.
- Landsberg, H. E. (1981). *The urban climate*. Academic press. :.
- Lebanon, R.o. (2016). *Lebanon's Third National Communication to the UNFCCC*. Retrieved from Beirut, Lebanon.
- Li, X.-X., & Norford, L. K. (2016). Evaluation of cool roof and vegetations in mitigating urban heat island in a tropical city, Singapore. *Urban Climate*, 16, 59–74.
- Masson, V. (2000). A physically-based scheme for the urban energy budget in atmospheric models. *Boundary-layer meteorology*, 94(3), 357–397.
- Mirzaei, P. A. (2015). Recent challenges in modeling of urban heat island. *Sustainable cities and society*, 19, 200–206.
- MoE, U., GEF. (2012). *Technology Needs Assessment Report for Climate Change*. Retrieved from Beirut.
- Moigne, P. (2012). Surfex scientific documentation. In: Version.
- Nations, U. (2018). Revision of world urbanization prospects. *United Nations: New York, NY, USA*, 799.
- OEA. (2010). *Thermal Standards for Buildings in Lebanon 2010*. Retrieved from Beirut, Lebanon.
- Pechtold, S. B., Ph. Bougeault, J.M. Carriere, J. Cuxart, V. Ducrocq, C. Fischer, M. Georgelin, P. Hereil, J.-P. Lafore, C. Liouesse, C. Mari, I. Mallet, P. J. Mascart, V. Masson, J.-P. Pinty, E. Richard, K. Suhre, J. Stein, P. Tulet, and J. Vila-Guerau de Arellano. (2014). *The MESO-NH atmospheric simulation system: scientific documentation*. Retrieved from France.
- Pigeon, G., Legain, D., Durand, P., & Masson, V. (2007). Anthropogenic heat release in an old European agglomeration (Toulouse, France). *International Journal of Climatology: A Journal of the Royal Meteorological Society*, 27(14), 1969–1981.
- Raman, A. P., Abou Anoma, M., Zhu, L., Rephaeli, E., & Fan, S. (2014). Passive radiative cooling below ambient air temperature under direct sunlight. *Nature*, 515(7528), 540–544.
- Rizwan, A. M., Dennis, L. Y., & Chunho, L. (2008). A review on the generation, determination and mitigation of Urban Heat Island. *Journal of environmental sciences*, 20(1), 120–128.
- Sailor, D. J., & Lu, L. (2004). A top-down methodology for developing diurnal and seasonal anthropogenic heating profiles for urban areas. *Atmospheric environment*, 38 (17), 2737–2748.
- Santamouris, M. (2018). *Minimizing energy consumption, energy poverty and global and local climate change in the built environment: innovating to zero: causalities and impacts in a zero concept world*: Elsevier.
- Santamouris, M., Ding, L., & Osmond, P. (2019). Urban heat island mitigation. In. *Decarbonising the built environment* (pp. 337–355). Springer.
- Saroufin, A., & Otayek, E. (2019). *Analysis and interpret road traffic congestion costs in Lebanon*. Paper presented at the MATEC Web of Conferences.
- Trombe, F. (1975). Perspectives sur l'utilisation des rayonnements solaires et terrestres dans certaines régions du monde.
- TWC. Weather Underground. Retrieved from <https://www.wunderground.com/>, (retrieved on October 1, 2021).
- Ulmer, F.-G., & Balss, U. (2016). Spin-up time research on the weather research and forecasting model for atmospheric delay mitigations of electromagnetic waves. *Journal of Applied Remote Sensing*, 10(1), Article 016027.
- UN. (2020). World Population Prospects. Retrieved from <https://population.un.org>.
- Varner, J. F., Eldabagh, N., Volta, D., Eldabagh, R., & Foley, J. J. (2019). WPTherm: A Python Package for the Design of Materials for Harnessing Heat. *Journal of open research software*, 7.
- Yang, J., Pyrgou, A., Chong, A., Santamouris, M., Kolokotsa, D., & Lee, S. E. (2018). Green and cool roofs' urban heat island mitigation potential in tropical climate. *Solar Energy*, 173, 597–609.
- Zhai, Y., Ma, Y., David, S. N., Zhao, D., Lou, R., Tan, G., ... Yin, X. (2017). Scalable-manufactured randomized glass-polymer hybrid metamaterial for daytime radiative cooling. *Science*, 355(6329), 1062–1066.
- Zhao, D., Aili, A., Zhai, Y., Xu, S., Tan, G., Yin, X., & Yang, R. (2019). Radiative sky cooling: Fundamental principles, materials, and applications. *Applied Physics Reviews*, 6(2), Article 021306.